Optical simulation of the Yang-Baxter equation

Shuang-Wei Hu,[1] Kang Xue,[2] and Mo-Lin Ge[1,*]
[1]*Theoretical Physics Division, Chern Institute of Mathematics, Nankai University, Tianjin 300071, People's Republic of China*
[2]*Department of Physics, Northeast Normal University, Changchun, Jilin 130024, People's Republic of China*
(Received 4 December 2007; published 12 August 2008)

In this paper, several proposals of optically simulating Yang-Baxter equations have been presented. Motivated by the recent development of anyon theory, we apply Temperley-Lieb algebra as a bridge to recast a four-dimensional Yang-Baxter equation into its two-dimensional counterpart. In accordance with both representations, we find the corresponding linear-optical simulations, based on the highly efficient optical elements. Both the degrees of freedom of photon polarization and location are utilized as the qubit basis, in which the unitary Yang-Baxter matrices are decomposed into a combination of actions of basic optical elements.

DOI: 10.1103/PhysRevA.78.022319 PACS number(s): 03.67.Lx, 42.50.Ex, 05.50.+q, 05.30.Pr

I. INTRODUCTION

The Yang-Baxter equation (YBE) originated in solving the one-dimensional δ-interacting models [1] and the statistical models on lattices [2,3]. The importance of the YBE was further realized as a starting point for the quantum inverse scattering method [4]. It is well-known that YBE plays an important role in solving the integrable models in quantum field theory and exactly solvable models in statistical mechanics ([3] and references therein). In quantum field theory, the YBE describes the scattering of particles in (1+1) dimensions. The essence of the YBE is to factorize the scattering of three particles into successive two-body scattering processes. The YBE also plays an important role in completely integrable statistical models, whose solutions can be found by means of the nested Bethe ansatz [5].

Due to its importance, the YBE deserves thus to be tested experimentally. Measuring the spectrum of spin chain, which is at the root of the YBE, one can learn the structure of spinon and thus check the factorization of the YBE. For instance, Heisenberg spin-1/2 chain model has been probed experimentally through neutron scattering experiments and the spectrum coincides with the calculation based on the YBE [6]. However, the YBE only provides sufficient condition for the prediction of spectrum. So these experiments should be viewed as indirect check of the YBE. The direct verification is still an open question.

In order to keep the paper self-contained, we first explain the basic formula of the YBE. The Yang-Baxter matrix $\breve{R}$ is a $N^2\times N^2$ matrix acting on the tensor product space $\mathcal{V}\otimes\mathcal{V}$, where N is the dimension of $\mathcal{V}$. Such a matrix $\breve{R}$ satisfies the YBE

$$\breve{R}_{12}(u)\breve{R}_{23}\left(\frac{u+v}{1+\beta^2uv}\right)\breve{R}_{12}(v)=\breve{R}_{23}(v)\breve{R}_{12}\left(\frac{u+v}{1+\beta^2uv}\right)\breve{R}_{23}(u), \tag{1}$$

where $\breve{R}_{12}=\breve{R}\otimes\mathbb{1}$, $\breve{R}_{23}=\mathbb{1}\otimes\breve{R}$, u and v are spectral parameters, and $\beta^{-1}=ic$ (c is light velocity). Take the two spin-1/2 particles as an example. Acting on such a system, $\breve{R}$ is a $2^2\times 2^2$ matrix whose matrix elements are $\breve{R}_{ab,cd}$, $a,b,c,d=\uparrow$ (spin up), $\downarrow$ (spin down). If spin is conserved, some matrix elements may vanish. The physical meaning of $\breve{R}(u)$ is two-particle scattering matrix depending on the relative rapidity $\tanh^{-1}(\beta u)$. When we change the spectral parameters as $\beta u=(1-x)/(1+x)$, $\beta v=(1-y)/(1+y)$ and $\beta(u+v)/(1+\beta^2uv)=(1-xy)/(1+xy)$, we obtain another ordinary form of the YBE,

$$\breve{R}_{12}(x)\breve{R}_{23}(xy)\breve{R}_{12}(y)=\breve{R}_{23}(y)\breve{R}_{12}(xy)\breve{R}_{23}(x), \tag{2}$$

i.e., the spectral parameter in the middle $\breve{R}(xy)$ matrix being the product of the neighborhoods' spectral parameters. The asymptotic limit $\breve{R}(x\to 0)=b$ satisfies the braid relation

$$b_{12}b_{23}b_{12}=b_{23}b_{12}b_{23}. \tag{3}$$

This relation is diagrammatically represented in Fig. 1. For a given matrix b satisfying Eq. (3) we can retrieve the corresponding $\breve{R}(x)$ matrix via the procedure of Baxterization or Yang-Baxterization [7]. This procedure depends on the numbers of independent eigenvalues of matrix b. In particular, when a braid matrix b has two independent eigenvalues λ_1

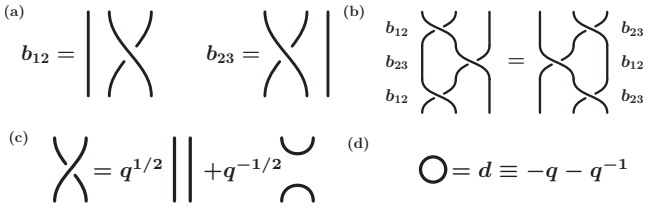

FIG. 1. (a) Diagrammatical interpretation of braid operators The labeled particle world lines, orienting from bottom to ceiling, are unaffected by smooth deformations in which the lines do not intersect. Each crossing means a scattering of two particles, including permutation process as the special case. (b) The braid relation (3) $b_{12}b_{23}b_{12}=b_{23}b_{12}b_{23}$. (c) Skein relation. (d) The unknotted loop. By skein relation we can eliminate all the crossings and get linear combinations of the Kauffman brackets for various disjoint unions of unknotted loops.

*geml@nankai.edu.cn

and λ_2, the corresponding $\check{R}(x)$ matrix obtained via Yang-Baxterization takes the form

$$\check{R}(x) = \rho(x)(b + x\lambda_1\lambda_2 b^{-1}), \tag{4}$$

where $\rho(x)$ is a normalization factor. For statistical models on lattice, the elements of $\check{R}(x)$ should be positive-definite, since they are related to the Boltzmann weights. However, as we will see below, there is no such restriction for the application to quantum entangled states.

In the recent years there is a new development to connect the braid matrix, as well as the YBE, with the entangled state [8–15]. The basic idea comes from the Bell states having the maximal entanglement degree. For a two-qubit system, Bell states are defined by

$$|\Phi^{\pm}\rangle = \frac{1}{\sqrt{2}}(|\uparrow\uparrow\rangle \pm |\downarrow\downarrow\rangle),$$

$$|\Psi^{\pm}\rangle = \frac{1}{\sqrt{2}}(|\uparrow\downarrow\rangle \pm |\downarrow\uparrow\rangle). \tag{5}$$

The Bell states are connected to the natural basis $|\Psi_0\rangle = (|\uparrow\uparrow\rangle, |\uparrow\downarrow\rangle, |\downarrow\uparrow\rangle, |\downarrow\downarrow\rangle)$ by a unitary transformation matrix W,

$$(|\Phi^-\rangle, |\Psi^+\rangle, |\Psi^-\rangle, |\Phi^+\rangle) = W(|\uparrow\uparrow\rangle, |\uparrow\downarrow\rangle, |\downarrow\uparrow\rangle, |\downarrow\downarrow\rangle),$$

$$W = \frac{1}{\sqrt{2}}\begin{pmatrix} 1 & 0 & 0 & 1 \\ 0 & 1 & -1 & 0 \\ 0 & 1 & 1 & 0 \\ -1 & 0 & 0 & 1 \end{pmatrix}. \tag{6}$$

(We refer the reader to [13] for more details about the short notation in the first line equation.) Kauffman *et al.* have shown that the matrix W is nothing but a braid matrix satisfying Eq. (3) by recognizing $\mathcal{V}$ as a two-dimensional complex vector space to hold a single qubit of information [9]. Further, it was found that W can be extended to matrix b such that [13]

$$b(q) = \frac{1}{\sqrt{2}}\begin{pmatrix} 1 & 0 & 0 & q \\ 0 & 1 & -1 & 0 \\ 0 & 1 & 1 & 0 \\ -q^{-1} & 0 & 0 & 1 \end{pmatrix} = \frac{1}{\sqrt{2}}(\mathbb{1} + M),$$

$$M^2 = -\mathbb{1}, \quad q = e^{i\phi}, \tag{7}$$

where real parameter ϕ is time-dependent flux. Yang-Baxterizing this braid matrix b, one can define a new state with arbitrary entanglement degree, as follows:

$$|\Psi(x,q)\rangle = \check{R}(x,q)|\Psi_0\rangle,$$

$$\check{R}(x,q) = \frac{1}{\sqrt{1+x^2}}[b(q) + xb(q)^{-1}], \tag{8}$$

where $\check{R}(x,q)$ matrix satisfies YBE (2) and meanwhile determines the evolution of the initial state $|\Psi_0\rangle$ to $|\Psi(x,q)\rangle$ given the time-dependent $q=q(t)$. In terms of the new variable $\cos\Theta = (1+x)/[\sqrt{2(1+x^2)}]$, $\check{R}(x,q)$ can be recast to

$$\check{R}(\Theta,\phi) = \begin{pmatrix} \cos\Theta & 0 & 0 & e^{-i\phi}\sin\Theta \\ 0 & \cos\Theta & -\sin\Theta & 0 \\ 0 & \sin\Theta & \cos\Theta & 0 \\ -e^{i\phi}\sin\Theta & 0 & 0 & \cos\Theta \end{pmatrix}. \tag{9}$$

It is interesting to observe that $\check{R}(\Theta,\phi)$ satisfies to the relation

$$\check{R}(\Theta,\phi) = \cos\Theta\mathbb{1} + \sin\Theta\mathrm{M}, \quad \mathrm{M}^2 = -\mathbb{1}, \tag{10}$$

i.e., as the extension of the Euler formula. When $\Theta=\pi/4$, $\check{R}(\Theta,\phi)$ reduces to b in Eq. (7), i.e., yielding the maximum of entangled states. When Θ takes other values the state $|\Psi(\Theta,\phi)\rangle = \check{R}(\Theta,\phi)|\Psi_0\rangle$ processes a continuous entanglement degree determined by Θ which is usually less than the maximum [13]. Suppose only the flux ϕ depends on t and under the adiabatic approximation, then we can obtain the Berry phase related to the YBE [13].

The theory sounds reasonable, but why we prefer to choose a Yang-Baxterized matrix $\check{R}(\Theta,\phi)$ as the unitary evolution is just an assumption. Especially, one may doubt the necessity of introducing the third particle to describe two-particle entanglement. We have to present a practical scheme to test the YBE in the framework of quantum information. Fortunately, there have been popular optical operations for the quantum gates [16] that are available to experimentally test the validity of such a YBE. The motivation of this paper is to propose a linear optical simulation of the YBE based on the highly efficient optical elements.

Both the braid matrix B in Eq. (7) and the $\check{R}(x)$ matrix in Eq. (9) act on the tensor product space $\mathcal{V}\otimes\mathcal{V}$ and thus have the four-dimensional (4D) representation. The entangled state in Eq. (8) requires that the optical simulation of the corresponding $\check{R}$ matrix involves the universal entangled gate, i.e., CNOT (=controlled-NOT) gate. In principle CNOT gates make use of measurement-induced nonlinearity and are still of low efficiency by means of optics [16,17]. The situation becomes worse when several sequent CNOT gates are involved. We have to find alternative ways to avoid this difficulty. Fortunately, as we will see in Sec. II, the 4D Yang-Baxter matrices have two-dimensional (2D) counterparts which are unitary and have much simpler realization by means of linear optics.

The paper is organized as follows. In Sec. II, we first prove the equivalence between 4D braid matrix and 2D braid matrix, then find the Yang-Baxterization procedure for the 2D braid matrix. Based on this theoretical assertion the optical test of the 2D YBE will be presented in Sec. III. A direct test of the 4D YBE is shown in Sec. IV. The conclusion is made in the Sec. V. The relationship between the basic for 2D braid matrices and 4D ones will be given in Appendix A.

II. TWO TYPES OF YBES

In the topological quantum computation theory, the 2D braid behavior under the exchange of anyons [18] has been investigated based on the $\nu=5/2$ fractional quantum Hall effect (FQHE) [15]. Motivated by this interesting application of braid relation in anyon theory, we will nest Temperley-Lieb algebra [19] into the 4D YBE and reduce it to a 2D YBE. Here we briefly present such an equivalence between these types of YBEs.

Let us first recall the braid behavior in $\nu=5/2$ FQHE. Quasiparticles in such a system are often called Ising anyons or $SU(2)_2$ states, which satisfy non-Abelian fractional statistics. There are three types of anyons, which can be called 0, $\frac{1}{2}$, 1. When two anyons become close together while other anyons are much farther away, these two anyons can be treated as a single particle whose quantum numbers are obtained by combining the original quantum numbers. For $SU(2)_2$ states, such a formation of new anyons obeys the following fusion rules:

$$\frac{1}{2}\times\frac{1}{2}=0+1,\quad \frac{1}{2}\times 1=\frac{1}{2},\quad 1\times 1=0,$$

$$0\times 0=0,\quad 0\times\frac{1}{2}=\frac{1}{2},\quad 0\times 1=1. \tag{11}$$

[These fusion rules are analogous to the decomposition rules for tensor products of irreducible SU(2) representations, but have an important difference that 1 is the maximum spin.] Note that there are two different fusion channels for two $\frac{1}{2}$ anyons. As a result, when four $\frac{1}{2}$ anyons fuse together to give 0, there is a two-dimensional space of such states. This can be done by dividing the four $\frac{1}{2}$ anyons into two pairs. Both pairs either fuse to 0 or to 1 then fuse the resulting anyons together to form 0. The orthogonal basis states read [15]

$|e_1\rangle =$ 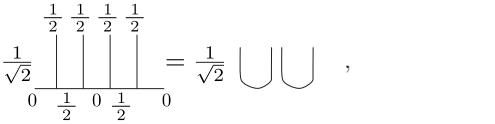 ,

$|e_2\rangle =$  . (12)

In the middle fusion chains (called conformal block), the internal edges are subject to the fusion rules at each trivalent vertex. In such conformal block basis, exchanging anyons is identified as braiding in Fig. 1. From the conformal basis to the Kauffman graph in the right-hand sides, Jones-Wenzl projector operators have been applied, i.e.

$\Pi_0 =$ 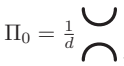 , $\Pi_1 =$ 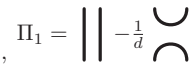 , (13)

where $d=\sqrt{2}$ in present case. By means of skein relation in Fig. 1, one can introduce the braid operators A and B which have nontrivial action on $|e_1\rangle$ and $|e_2\rangle$,

$A|e_1\rangle =$

$A|e_2\rangle =$ 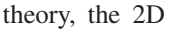

$B|e_1\rangle =$ 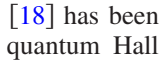

$B|e_2\rangle =$ 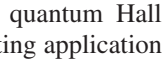 (14)

Thus their matrix representations in the basis $(|e_1\rangle,\ |e_2\rangle)$ are given by

$$A=e^{-i\pi/8}\begin{pmatrix}1 & 0\\ 0 & i\end{pmatrix},$$

$$B=\frac{e^{-i\pi/8}}{2}\begin{pmatrix}1+i & 1-i\\ 1-i & 1+i\end{pmatrix}, \tag{15}$$

and they satisfy the two-dimensional braid relation

$$ABA=BAB. \tag{16}$$

We emphasize that Eq. (16) acts on the basis $(|e_1\rangle,\ |e_2\rangle)$. It is worthy of noting that the "crossing" in Eq. (14) means the usual 4×4 braid matrix, satisfying Eq. (3). These braid matrices A and B are unitary and have a natural realization by linear optics, as we will see in Sec. III.

In order to generalize the above procedure from braid relation to YBE, we nest Temperley-Lieb algebra [19] into the 4D YBE and surprisingly reduce it to a 2D YBE. Detailed calculations will be given later (see Appendix A). Briefly, acting on the subspace spanned by $|e_1\rangle$ and $|e_2\rangle$, the 4D YBE (1) will reduce to the corresponding 2D YBE,

$$A(u)B\left(\frac{u+v}{1+\beta^2uv}\right)A(v)=B(v)A\left(\frac{u+v}{1+\beta^2uv}\right)B(u),$$

$$A(u)=\rho(u)\begin{pmatrix}\dfrac{1+\beta^2u^2+2i\epsilon\beta u}{1+\beta^2u^2-2i\epsilon\beta u} & 0\\ 0 & 1\end{pmatrix},$$

$$B(u)=\frac{\rho(u)}{1+\beta^2u^2-2i\epsilon\beta u}\begin{pmatrix}1+\beta^2u^2 & 2i\epsilon\beta u\\ 2i\epsilon\beta u & 1+\beta^2u^2\end{pmatrix}, \tag{17}$$

where $\rho(u)$ is the normalization factor and $\epsilon=\pm 1$. Since these matrices $A(u)$ and $B(u)$ are unitary, it is obviously easier to optically simulate this 2D equation than the previous 4D edition. For the convenience of experimental check, we further introduce the transformation

$$\frac{1+\beta^2u^2+2i\epsilon\beta u}{1+\beta^2u^2-2i\epsilon\beta u}\equiv e^{-2i\theta},\quad \rho(u)\equiv e^{i\theta}, \tag{18}$$

then we obtain the following form of SU(2) matrices:

$$A(u)=\begin{pmatrix}e^{-i\theta} & 0\\ 0 & e^{i\theta}\end{pmatrix}\equiv A(\theta),$$

$$B(u)=\begin{pmatrix}\cos\theta & -i\sin\theta\\ -i\sin\theta & \cos\theta\end{pmatrix}\equiv B(\theta). \tag{19}$$

In terms of this new parameter, the solution of the $\check{R}(\theta)$ matrix takes the form

$$\breve{R}(\theta,\phi)=\begin{pmatrix} \cos\theta & 0 & 0 & e^{-i\phi}\sin\theta \\ 0 & \cos\theta & -\sin\theta & 0 \\ 0 & \sin\theta & \cos\theta & 0 \\ -e^{i\phi}\sin\theta & 0 & 0 & \cos\theta \end{pmatrix}. \tag{20}$$

Though it takes the similar form with Eq. (9), the parameter θ has different meaning from the parameter Θ. One may wonder where is the missing parameter ϕ in the 2D YBE. It actually survives in the basis $|e_1\rangle$ and $|e_2\rangle$ which the 2D YBE should act on (see the explicit form of the basis in Appendix A).

These two unitary matrices can be optically realized with the aid of the "polarization qubit" or "location qubit" of a single photon. In the following we present two experimental setups to simulate the YBE by means of these two ways.

III. OPTICAL SIMULATION OF 2D YBE

The single-photon representation of qubits plays an important role in linear optical computation [20–22]. The key is that a single photon can be utilized to act both as polarization qubit and as location qubit. For the former one encodes the qubit in the photon's polarization with the corresponding transformations simulated by wave plates, such as half-wave plates (HWPs) and quarter-wave plates (QWPs). For the latter, one encodes the qubit in the single-photon paths with the corresponding transformations simulated by beam splitters (BSs), phase shifters (PSs), and mirrors. As a result, universal unitary gates (1-qubit or 2-qubit) can be realized by means of either of these two kinds of qubit transformation, or by combining both [20,21].

The two unitary matrices in Eq. (19) can be optically realized with the aid of the "polarization qubit" or "location qubit" of a single photon. In the following we present two experimental setups to simulate the YBE by means of these two ways.

A. Using polarization qubit to simulate 2D YBE

We first recall the action of a QWP upon the basis states of the polarization qubit [22]

$$U_Q(\delta)=e^{-i\delta\sigma_2}e^{-i(\pi/4)\sigma_3}e^{i\delta\sigma_2}=\frac{1}{\sqrt{2}}\begin{pmatrix} 1-i\cos(2\delta) & -i\sin(2\delta) \\ -i\sin(2\delta) & 1+i\cos(2\delta) \end{pmatrix}, \tag{21}$$

where σ_i are Pauli matrices and δ is the angle between the QWP axis and the vertical direction. Then the action of a HWP upon the basis states of the polarization qubit is given by

$$U_H(\delta)=U_Q^2(\delta)=-i\begin{pmatrix} \cos(2\delta) & \sin(2\delta) \\ \sin(2\delta) & -\cos(2\delta) \end{pmatrix}. \tag{22}$$

As an analog with Euler rotation, the sandwich configuration of one HWP and two QWPs enables one to perform any unitary changes of the photons polarization state [23]. Particularly, for the case in Eq. (19), we obtain

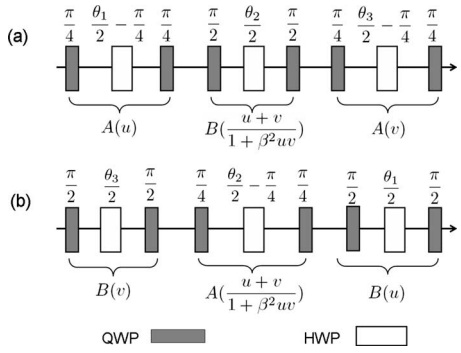

FIG. 2. Schematic setup for simulating either side of 2D YBE (17) by means of a polarization qubit. The angle parameters θ_i are determined by Eq. (25) while the relations between θ_i and u, v are determined by Eq. (24).

$$A(\theta)=U_Q\left(\frac{\pi}{4}\right)U_H\left(-\frac{\pi}{4}+\frac{\theta}{2}\right)U_Q\left(\frac{\pi}{4}\right),$$

$$B(\theta)=U_Q\left(\frac{\pi}{2}\right)U_H\left(\frac{\theta}{2}\right)U_Q\left(\frac{\pi}{2}\right). \tag{23}$$

By this decomposition it is straightforward to design the experimental setup for simulation of a two-dimensional YBE (17). As Fig. 2 shows, a suitable series of QWPs and HWPs with different direction angles in succession will simulate the left-hand side (LHS) of YBE while another series will do the right-hand side (RHS). In Fig. 2, the relation (18) requires the angle parameters θ_i in the LHS satisfy

$$\frac{1-\beta^2u^2+2i\epsilon\beta u}{1-\beta^2u^2-2i\epsilon\beta u}=e^{-2i\theta_1},$$

$$\frac{1-\beta^2\left(\frac{u+v}{1+\beta^2uv}\right)^2+2i\epsilon\beta\frac{u+v}{1+\beta^2uv}}{1-\beta^2\left(\frac{u+v}{1+\beta^2uv}\right)^2-2i\epsilon\beta\frac{u+v}{1+\beta^2uv}}=e^{-2i\theta_2},$$

$$\frac{1-\beta^2v^2+2i\epsilon\beta v}{1-\beta^2v^2-2i\epsilon\beta v}=e^{-2i\theta_3}. \tag{24}$$

Thus we have

$$(e^{-2i\theta_2}+1)[i-\sec(\theta_1-\theta_3)\sin(\theta_1+\theta_3)]=2i. \tag{25}$$

This also holds for the angle parameters appearing in the RHS of YBE (17). What we should measure in experiment is the actions of transformation of both sides given the input states with the same angle parameters, for example, by means of quantum state tomography [24].

B. Using location qubit to simulate 2D YBE

When we take photon location paths as qubit basis, the unitary transformations can be achieved by means of BSs and PSs. We follows the notations in [20] which are different from those in [21], especially the opposite definitions of location qubit lead to distinct actions of mirror. First, we list the actions of several elementary gates on the location qubit basis (see Fig. 3)

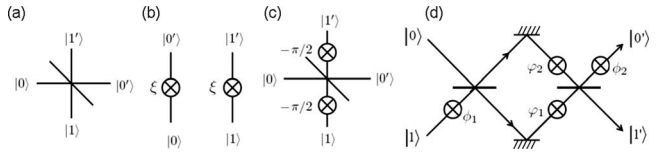

FIG. 3. Gates acting on location qubit basis: (a) Beam splitter U_{BS}. (b) Phase shifters $U^0_{PS}(\xi)$ (left) and $U^1_{PS}(\xi)$ (right). (c) Hadamard gate H by a 50:50 BS and two $-\pi/2$ PS. (d) Mach-Zehnder interferometer U_{MZ} as a universal 1-qubit gate. For simplicity, each pair of $-\pi/2$ phase shifters accompanied with every beam splitter as in (c) is not shown in (d).

$$U_{BS} = \frac{1}{\sqrt{2}}\begin{pmatrix} 1 & i \\ i & 1 \end{pmatrix},$$

$$U_{mirr} = \mathbb{1}_2,$$

$$U^0_{PS}(\xi) = \begin{pmatrix} e^{i\xi} & 0 \\ 0 & 1 \end{pmatrix},$$

$$U^1_{PS}(\xi) = \begin{pmatrix} 1 & 0 \\ 0 & e^{i\xi} \end{pmatrix},$$

$$H = U^1_{PS}\left(-\frac{\pi}{2}\right)U_{BS}U^1_{PS}\left(-\frac{\pi}{2}\right) = \frac{1}{\sqrt{2}}\begin{pmatrix} 1 & 1 \\ 1 & -1 \end{pmatrix}. \quad (26)$$

Based on these gates, a Mach-Zehnder interferometer [Fig. 3(d)] can realize arbitrary U(2) group element [20,21]. Note that in Fig. 3(d) each pair of $-\pi/2$ phase shifters accompanied with every beam splitter is not shown for simplicity. We hold this convention hereafter, so each BS should be taken as a Hadamard gate. The unitary action of Mach-Zehnder interferometer is given by

$$U_{MZ} = U^1_{PS}(\phi_1)HU_{mirr}U^1_{PS}(\varphi_2)U^0_{PS}(\varphi_1)HU^0_{PS}(\phi_2) = e^{i\Phi/2}\begin{pmatrix} e^{-i\phi_1-\phi_2/2}\cos\frac{\lambda}{2} & ie^{i\phi_1-\phi_2/2}\sin\frac{\lambda}{2} \\ ie^{-i\phi_1-\phi_2/2}\sin\frac{\lambda}{2} & e^{i\phi_1-\phi_2/2}\cos\frac{\lambda}{2} \end{pmatrix}, \quad (27)$$

where the total phase $\Phi = \phi_1 + \phi_2 + \varphi_1 + \varphi_2$ and phase difference $\lambda = \varphi_2 - \varphi_1$. Through Mach-Zehnder interferometer, we can perform the action of operators A and B in Eq. (23) with angles correspondences as

$$A(\theta) = U_{MZ}(\varphi_2 = \varphi_1 = 0,\ \ \phi_1 = -\phi_2 = \theta) = U^0_{PS}(-\theta)U^1_{PS}(\theta),$$

$$B(\theta) = U_{MZ}(\varphi_2 = -\varphi_1 = \theta,\ \ \phi_1 = \phi_2 = 0). \quad (28)$$

Then we come to the whole optical setup to simulate both sides of the 2D YBE, Eq. (17), as shown in Fig. 4. The angle parameters obey the same relation in Eq. (25).

IV. OPTICAL SIMULATION OF FOUR-DIMENSIONAL YBE

The YBE in four dimension representation (1) is equivalent to

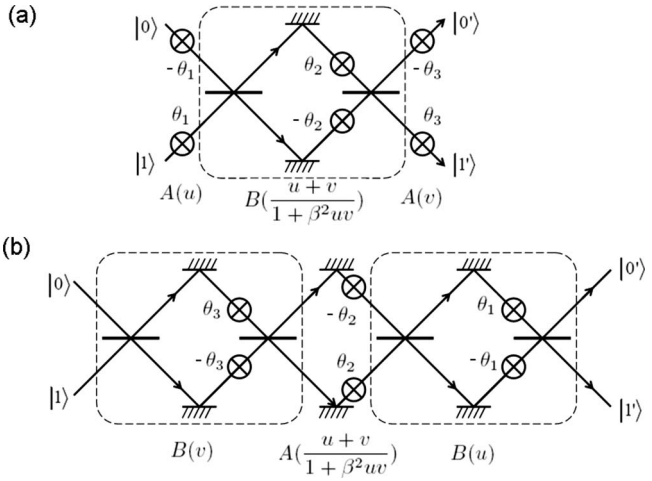

FIG. 4. Schematic setup for simulating either side of 2D YBE (17) by means of location qubit. (a) Simulation of LHS. (b) Simulation of RHS. Each pair of $-\pi/2$ phase shifters accompanied with every beam splitter is not shown. The relations of different parameters are refereed to Eq. (25).

$$[\breve{R}(\theta_1)\otimes\mathbb{1}_2]\cdot[\mathbb{1}_2\otimes\breve{R}(\theta_2)]\cdot[\breve{R}(\theta_3)\otimes\mathbb{1}_2] = [\mathbb{1}_2\otimes\breve{R}(\theta_3)]\cdot[\breve{R}(\theta_2)\otimes\mathbb{1}_2]\cdot[\mathbb{1}_2\otimes\breve{R}(\theta_1)], \quad (29)$$

where θ_i satisfy the relation (25) and $\breve{R}(\theta)$ takes the form in Eq. (20). The $\breve{R}(\theta)$ matrix can be decomposed into the combination of elementary gates [25]. The case $\theta=0$ is trivial. When $\theta=\pi/4$ or $3\pi/4$ [we restrict $\theta\in(0,2\pi)$], $\breve{R}(\theta)$ reduces to the braid matrix (7) and thus equivalent to one CNOT gate, as Kauffman *et al.* first pointed out [9]. When θ takes other values, it can decomposed as follows:

$$\breve{R}(\theta) = (V_1\otimes V_2)\cdot\text{CNOT2}\cdot(V_3\otimes V_4)\cdot\text{CNOT2}\cdot(V_5\otimes V_6), \quad (30)$$

where $V_i\in\mathrm{U}(2)$ and CNOT2 gate is given by

$$\text{CNOT2} = \begin{pmatrix} 1 & 0 & 0 & 0 \\ 0 & 0 & 0 & 1 \\ 0 & 0 & 1 & 0 \\ 0 & 1 & 0 & 0 \end{pmatrix}. \quad (31)$$

Below we focus on the general case, i.e., $\theta\neq 0$, $\pi/4$, or $3\pi/4$. Recently, Bullock and his coauthors [26] have developed a criterion for determining the number of CNOT (or equivalently CNOT2) gates to simulate a given transformation. By this criterion, one can check that the decomposition (30) is optimal, i.e., the $\breve{R}(\theta)$ matrix admits a quantum circuit using 2 CNOT gates (see Appendix C).

Detailed calculation (see Appendix C) further shows $V_i\in\mathrm{SU}(2)$ for the present case. More explicitly, we have

$$V_1 = \frac{1}{\sqrt{2}}\begin{pmatrix} e^{-i\pi+\phi/4} & e^{-i\pi+\phi/4} \\ -e^{i\pi+\phi/4} & e^{i\pi+\phi/4} \end{pmatrix},$$

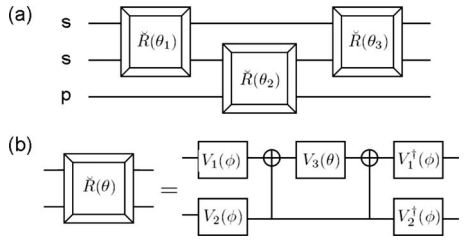

FIG. 5. (a) A circuit for simulating the left-hand side of four-dimensional YBE (1), with s and p denoting location and polarization qubit channels, respectively. (b) The decomposition of $\check{R}(\theta)$ matrix, see Eq. (30).

$$V_2 = \frac{1}{\sqrt{2}}\begin{pmatrix} e^{-i\phi/4} & -e^{-i\phi/4} \\ e^{i\phi/4} & e^{i\phi/4} \end{pmatrix},$$

$$V_3 = \begin{pmatrix} e^{-i\theta} & 0 \\ 0 & e^{i\theta} \end{pmatrix},$$

$$V_4 = \mathbb{1}_2, \quad V_5 = V_1^\dagger, \quad V_6 = V_2^\dagger. \tag{32}$$

By this explicit decomposition (30), the design of the circuit to simulate YBE is straightforward, as shown in Fig. 5. The difficulty lies in realization of the CNOT gates. As is described in a previous section, a photon can carry either "polarization qubit" or "location qubit." If we only use the former, CNOT gates are possible for photons in principle using measurement-induced nonlinearity [27]. However, currently they are still low-efficient and experimentally expensive [16,17]. For the present status of linear optics experiments, it was shown that the success probability of an array of n CNOT gates can be made to operate with a probability of $p=(\frac{1}{3})^{n+1}$ [28]. The above decomposition of $\check{R}(\theta)$ takes 2 CNOT2 gates. For each side of YBE (5), we have to deal with 6 CNOT gates at the same time. Thus the success probability is $p=(\frac{1}{3})^7 \simeq 4.57\times 10^{-4}$, which makes the practical simulation extremely difficult. This is the reason why we did map the 4D YBE to 2D YBE.

A photon used as a location qubit will help reduce the above difficulty when we do a small-scale quantum calculation. The key lies in the high efficiency of BSs, PSs, and wave plates. In Fig. 5 we have to deal with three qubit, then two schemes are available: one polarization qubit channel plus two location qubit channels, or all location qubit channels. We focus on the former since it saves one optical way and uses a less number of beam splitters.

In Fig. 5(a), three channels are designed to be location (s), location (s), and polarization (p) qubits from top to floor. For polarization qubit, using the QWPs and HWPs, the unitary matrices V_i can be decomposed into

$$V_1 = U_Q\left(\frac{\pi}{4}\right)U_H\left(\frac{\phi}{8}\right)U_Q\left(\frac{\pi}{2}\right),$$

$$V_2 = U_Q\left(-\frac{\pi}{4}\right)U_H\left(\frac{\pi-\phi}{8}\right)U_Q\left(\frac{\pi}{2}\right),$$

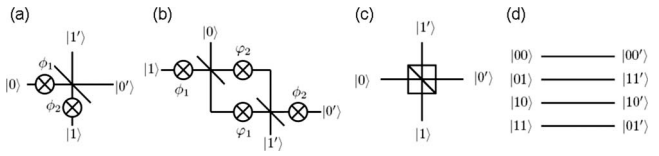

FIG. 6. (a) The realization of U_1 acting on location qubit with $\phi_1=-\frac{\pi+\phi}{4}$ and $\phi_2=\frac{5\pi+\phi}{4}$. (b) The realization of U_2 acting on location qubit with $\phi_1=\frac{\pi}{2}$, $\phi_2=\frac{\pi-\phi}{2}$, $\varphi_1=\frac{\phi-\pi}{4}$, and $\varphi_2=\frac{\phi-3\pi}{4}$. (c) CNOT2 gate using a polarizing beam splitter with the polarization and location being the control and target qubit, respectively. (d) CNOT2 gate between location qubits, which is achieved by swapping the labels of output paths $|01\rangle$ and $|11\rangle$.

$$V_2^\dagger = U_Q(0)U_H\left(\frac{5\pi-\phi}{8}\right)U_Q\left(\frac{\pi}{4}\right),$$

$$V_3 = U_Q\left(\frac{\pi}{4}\right)U_H\left(\frac{2\theta-\pi}{4}\right)U_Q\left(\frac{\pi}{4}\right). \tag{33}$$

For the location qubit, as the previous section shows, a Mach-Zehnder interferometer can simulate these V_i matrices. We summarize the results in Figs. 6(a) and 6(b).

The rest come to two types of CNOT2 gates: one is between location qubit and polarization qubit, the other is between two location qubits. For the former, it can be achieved by a polarizing beam splitter where the location qubit is flipped or not conditionally on its state of polarization, as shown in Fig. 6(c) [20]. For the latter, the two location qubits in Fig. 6(d) correspond to the first and second number of the binary representation of the location of a single photon, respectively. Thus the corresponding CNOT2 is simulated by simply swapping the labels of path $|10\rangle$ and $|11\rangle$ [see Fig. 6(d)].

Gathering all the elementary gates, we finally arrive at the whole scheme for optically simulating the LHS of the 4D YBE, as shown in Fig. 7. In order to get the optical setup to simulate the RHS of the 4D YBE, we can apply the formal equivalence between two hand sides in the YBE (1) by cycling the indices $1\to 2$, $2\to 3$, $3\to 1$ and exchanging the parameters $u\leftrightarrow v$. The equality will be confirmed by means of tomography given the same input on each sides.

V. CONCLUSION

We have presented several proposals to optically simulate Yang-Baxter equations. According to the development of theoretical analysis, a Yang-Baxter equation in two-dimensional representation and in four-dimensional representation can be uniformed with the aid of Temperley-Lieb algebra. In both representations, we have found the corresponding linear-optical realizations, based on the highly efficient optical elements, i.e., half-wave plates, quarter-wave plates, beam splitters, phase shifters, and mirrors. Both the degrees of freedom of photon polarization and location have been utilized as the qubit basis. In each kind of basis, the unitary Yang-Baxter matrices have been decomposed into combination of actions of basic optical elements. The developed proposals, in principle, are able to be used to directly

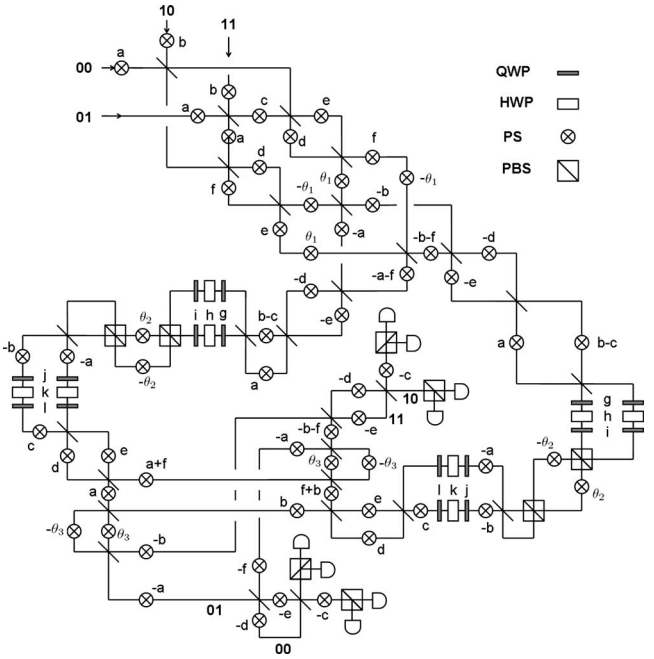

FIG. 7. The whole optical setup of simulating the LHS of the 4D YBE shown in Fig. 5. The binary numbers indicate location qubit basis. Each pair of $-\pi/2$ phase shifters accompanied with every beam splitter is not shown. The phase shifts of other PSs, from a to f, are $-(\pi+\phi)/4$, $(5\pi+\phi)/4$, $\pi/2$, $(\phi-\pi)/4$, $(\phi-3\pi)/4$, and $(\pi-\phi)/2$, respectively. The angles of wave plates to form U_2 and $U_2^\dagger$, from g to l, are $\pi/2$, $(\pi-\phi)/8$, $-\pi/4$, $\pi/4$, $(5\pi-\phi)/8$, and 0, respectively [see Eq. (33)]. Mirrors are placed on every corner.

check the Yang-Baxter equation. We remark that the test of the 2D YBE is, in fact, to provide an optical simulation of two-component anyons associated with FQHE. The anyon behavior is now a hot topic [15], but to our knowledge there has not been a scheme to test by using an optical simulation.

ACKNOWLEDGMENTS

The authors would like to thank Professor J. L. Chen, Professor X. Wan, M. G. Hu, B. X. Xie, and M. S. Li for their useful discussions. This work was supported in part by NSF of China (Grant No. 10575053) and Liu Hui Center of Nankai and Tianjin Universities.

APPENDIX A: REDUCTION OF 4D YBE

Analog with the mapping from 4D braid relation to 2D braid relation in Sec. II, we here give the calculation of their Yang-Baxterized edition. This is equivalent to Yang-Baxterize (16). First we recall the involved YBE,

$$\check{R}_{12}(u)\check{R}_{23}\left(\frac{u+v}{1+\beta^2uv}\right)\check{R}_{12}(v)=\check{R}_{23}(v)\check{R}_{12}\left(\frac{u+v}{1+\beta^2uv}\right)\check{R}_{23}(u). \tag{A1}$$

What is interesting is that this four-dimensional YBE (A1) admits the celebrated Temperley-Lieb algebra (TLA). Actually set

$$\check{R}_{12}(u)=a_1(u)\mathbb{1}_6+b_1(u)U_{12},$$

$$\check{R}_{23}(u)=a_2(u)\mathbb{1}_6+b_2(u)U_{23}, \tag{A2}$$

and suppose U satisfying TLA [19]

$$U^2=dU,\quad U_{12}U_{23}U_{12}=U_{12},\quad U_{23}U_{12}U_{23}=U_{23}, \tag{A3}$$

where d is the loop in Fig. 1, taking the value of $\sqrt{2}$ in our case. The coefficient functions $a_i(u)$ and $b_j(u)$ in Eq. (A2) are determined by the associated YBE (A1). Consider one simple but important case: $a_1(u)=a_2(u)=a(u)$ and $b_1(u)=b_2(u)=b(u)$. We easily get

$$[a(u)b(v)+b(u)a(v)+db(u)b(v)]a\left(\frac{u+v}{1+uv}\right)$$

$$=[a(v)a(u)-b(v)a(u)]b\left(\frac{u+v}{1+uv}\right). \tag{A4}$$

Equation (A4) has the solution

$$a(u)=\rho(u),\quad b(u)=\rho(u)G(u),$$

$$G(u)=\frac{4i\epsilon\beta u}{\sqrt{2}(1+\beta^2u^2-2i\epsilon\beta u)}\quad(\epsilon=\pm 1). \tag{A5}$$

On the other hand, in accordance with Eqs. (13) and (14), the new basis $|e_i\rangle(i=1,2)$ is introduced from the definition of the operator U,

$$U_{12}|e_1\rangle=U_{34}|e_1\rangle=d|e_1\rangle,$$

$$U_{12}|e_2\rangle=U_{34}|e_2\rangle=0,$$

$$U_{23}|e_1\rangle=U_{14}|e_1\rangle=\frac{1}{d}(|e_1\rangle+\sqrt{d^2-1}|e_2\rangle),$$

$$U_{23}|e_2\rangle=U_{14}|e_2\rangle=\frac{\sqrt{d^2-1}}{d}(|e_1\rangle+\sqrt{d^2-1}|e_2\rangle). \tag{A6}$$

Thus we have

$$\check{R}_{12}(u)|e_1\rangle=[a_1(u)+d\ \ b_1(u)]|e_1\rangle,$$

$$\check{R}_{12}(u)|e_2\rangle=a_1(u)|e_2\rangle,$$

$$\check{R}_{23}(u)|e_1\rangle=\left[a_2(u)+\frac{b_2(u)}{d}\right]|e_1\rangle+\frac{\sqrt{d^2-1}}{d}b_2(u)|e_2\rangle,$$

$$\check{R}_{23}(u)|e_2\rangle=\frac{\sqrt{d^2-1}}{d}b_2(u)|e_1\rangle+\left[a_2(u)+\frac{d^2-1}{d}b_2(u)\right]|e_2\rangle. \tag{A7}$$

So $|e_1\rangle$ and $|e_2\rangle$ span the $\check{R}$-invariant subspace. Then it is natural to define the matrix elements $A(u)_{ij}=\langle e_i|\check{R}_{12}(u)|e_j\rangle$ and $B(u)_{ij}=\langle e_i|\check{R}_{23}(u)|e_j\rangle$.

Combing the above results we obtain the explicit form of $A(u)$ and $B(u)$,

$$A(u) = \rho(u)\begin{pmatrix} \dfrac{1+\beta^2u^2+2i\epsilon\beta u}{1+\beta^2u^2-2i\epsilon\beta u} & 0 \\ 0 & 1 \end{pmatrix},$$

$$B(u) = \frac{\rho(u)}{1+\beta^2u^2-2i\epsilon\beta^2u}\begin{pmatrix} 1+\beta^2u^2 & 2i\epsilon\beta u \\ 2i\epsilon\beta u & 1+\beta^2u^2 \end{pmatrix}, \quad \text{(A8)}$$

and importantly, in accord with the braid relation (16), they satisfy the two-dimensional (2D) YBE

$$A(u)B\left(\frac{u+v}{1+uv}\right)A(v) = B(v)A\left(\frac{u+v}{1+uv}\right)B(u). \quad \text{(A9)}$$

The corresponding unitary matrix U with $d=\sqrt{2}$, which satisfies TLA in Eq. (A3), takes the representation

$$U = \frac{1}{\sqrt{2}}\begin{pmatrix} 1 & 0 & 0 & iq^{-1} \\ 0 & 1 & i\epsilon & 0 \\ 0 & -i\epsilon & 1 & 0 \\ -iq & 0 & 0 & 1 \end{pmatrix} = \frac{1}{\sqrt{2}}(\mathbb{1}+iM),$$

$$M^2 = -\mathbb{1}, \quad q = e^{i\phi}, \quad \phi \in \mathbb{R}. \quad \text{(A10)}$$

Here the important factor i before matrix M distinguishes U from the braid operator in Eq. (7). In terms of new parameters as in Eq. (18), the explicit form of $\check{R}(\theta)$ takes

$$\check{R}(\theta) = a(u) + b(u)U = \rho(u)[\mathbb{1}_4 + G(u)U] = \begin{pmatrix} \cos\theta & 0 & 0 & e^{-i\phi}\sin\theta \\ 0 & \cos\theta & -\sin\theta & 0 \\ 0 & \sin\theta & \cos\theta & 0 \\ -e^{i\phi}\sin\theta & 0 & 0 & \cos\theta \end{pmatrix}. \quad \text{(A11)}$$

By setting $a=\rho$ and $b=\rho p$, where $p=\frac{1}{2}(-d\pm\sqrt{d^2-4})$ with $d=\sqrt{2}$, i.e., $p=-\exp(\pm i\pi/4)$, we regain A and B matrices as in Eq. (15), which satisfy the braid relation (16). This result can be also obtained through the "light-cone" limit of Eq. (A1) by setting three arguments in $\check{R}$-matrices to be equal, i.e.,

$$u = v = \frac{u+v}{1+\beta^2uv}, \quad \text{(A12)}$$

which is satisfied by either $u=v=0$ or $u=v=\beta^{-1}$. Under the limit in Eq. (A12), $A(u)$ and $B(u)$ reduce to Eq. (15).

We know that by taking $Q\equiv iq^{-1}=i$ [i.e., $Q^4=1$], the U matrix given by Eq. (A10) becomes

$$U(Q=i) = \frac{1}{\sqrt{2}}\begin{pmatrix} 1 & 0 & 0 & i \\ 0 & 1 & i & 0 \\ 0 & -i & 1 & 0 \\ -i & 0 & 0 & 1 \end{pmatrix}, \quad \text{(A13)}$$

which is the transformation matrix for the Bell states [10]. We thus conclude that the four-dimensional entangling braid matrix (A13) and the two-dimensional braid matrix (15) can be uniformed by acting the TLA operator on different dimensional basis. The four-dimensional basis can be $(|\uparrow\uparrow\rangle,|\uparrow\downarrow\rangle,|\downarrow\uparrow\rangle,|\downarrow\downarrow\rangle)$, whereas the logic qubit basis reads $(|e_1\rangle,|e_2\rangle)$. Conversely, the latter can be expanded in terms of four-spin states and thus relate with the four-dimensional basis. In order to find this correspondence, we first rewrite U_{ij} as a form of projectors

$$U_{ij} = \sqrt{2}(|\psi_{ij}\rangle\langle\psi_{ij}| + |\varphi_{ij}\rangle\langle\varphi_{ij}|), \quad \text{(A14)}$$

where

$$|\psi_{ij}\rangle = \frac{1}{\sqrt{2}}(|\uparrow\uparrow\rangle_{ij} + e^{-i\phi'}|\downarrow\downarrow\rangle_{ij}),$$

$$|\varphi_{ij}\rangle = \frac{1}{\sqrt{2}}(|\uparrow\downarrow\rangle_{ij} - i|\downarrow\uparrow\rangle_{ij}),$$

$$\phi' = -\left(\phi + \frac{3\pi}{2}\right). \quad \text{(A15)}$$

It is interesting that both $|\psi_{ij}\rangle$ and $|\varphi_{ij}\rangle$ are maximally entangled states for two spins, i.e., Bell states. With the aid of Eq. (A6), we arrive at

$$|e_1\rangle = \frac{1}{\sqrt{1+|\nu|^2}}(|\psi_{12}\rangle|\psi_{34}\rangle + \nu|\varphi_{12}\rangle|\varphi_{34}\rangle),$$

$$|e_2\rangle = \frac{1}{\sqrt{1+|\nu|^2}}[(1-i\nu e^{i\phi'})|\psi_{23}\rangle|\psi_{41}\rangle - \nu(1-i\nu^{-1}e^{-i\phi'})|\varphi_{23}\rangle|\varphi_{41}\rangle] - |e_1\rangle, \quad \text{(A16)}$$

with ν an arbitrary coefficient. A detailed calculation is shown in Appendix B.

Briefly, in the invariant subspace spanned by $|e_1\rangle$ and $|e_2\rangle$, the $\check{R}$ matrices satisfying the 4D YBE (A1) will reduce to the 2D representation, $A(u)$ and $B(u)$, with the corresponding 2D YBE (17).

APPENDIX B: CALCULATION FOR $|e_i\rangle$

Here we give the details of calculation for $|e_i\rangle$ $(i=1,2)$. We start from

$$U_{12}|e_1\rangle = U_{34}|e_1\rangle = d|e_1\rangle, \quad \text{(B1)}$$

$$U_{12}|e_2\rangle = U_{34}|e_2\rangle = 0, \quad \text{(B2)}$$

$$U_{23}|e_1\rangle = U_{14}|e_1\rangle = \frac{1}{d}(|e_1\rangle + \sqrt{d^2-1}|e_2\rangle), \quad \text{(B3)}$$

$$U_{23}|e_2\rangle = U_{14}|e_2\rangle = \frac{\sqrt{d^2-1}}{d}(|e_1\rangle + \sqrt{d^2-1}|e_2\rangle). \quad \text{(B4)}$$

Generally, $|e_i\rangle$ can be expanded into the linear combination of Bell states

$$|\psi_{ij}^{\pm}\rangle = \frac{1}{\sqrt{2}}(|\uparrow\uparrow\rangle_{ij} \pm e^{-i\phi'}|\downarrow\downarrow\rangle_{ij}),$$

$$|\varphi_{ij}^{\pm}\rangle = \frac{1}{\sqrt{2}}(|\uparrow\downarrow\rangle_{ij} \mp i|\downarrow\uparrow\rangle_{ij}). \tag{B5}$$

Due to the project form of U_{ij}

$$U_{ij} = \sqrt{2}(|\psi_{ij}^{+}\rangle\langle\psi_{ij}^{+}| + |\varphi_{ij}^{+}\rangle\langle\varphi_{ij}^{+}|), \tag{B6}$$

one can get the general expression of $|e_i\rangle$ from Eqs. (B1) and (B2),

$$\begin{aligned}|e_1\rangle = a_1|\psi_{12}^{+}\rangle|\psi_{34}^{+}\rangle + a_2|\psi_{12}^{+}\rangle|\varphi_{34}^{+}\rangle \\ + a_3|\varphi_{12}^{+}\rangle|\psi_{34}^{+}\rangle + a_4|\varphi_{12}^{+}\rangle|\varphi_{34}^{+}\rangle,\end{aligned}$$

$$\begin{aligned}|e_2\rangle = a_5|\psi_{12}^{-}\rangle|\psi_{34}^{-}\rangle + a_6|\psi_{12}^{-}\rangle|\varphi_{34}^{-}\rangle \\ + a_7|\varphi_{12}^{-}\rangle|\psi_{34}^{-}\rangle + a_8|\varphi_{12}^{-}\rangle|\varphi_{34}^{-}\rangle.\end{aligned} \tag{B7}$$

We further notice that Eqs. (B3) and (B4) indicate the symmetry of exchanging pair indices $23 \leftrightarrow 14$ for $|e_i\rangle$. Taking of this symmetry and noticing the minus sign in the expression of ψ_{ij}^{-} and φ_{ij}^{+}, we further simplify $|e_i\rangle$ into

$$\begin{aligned}|e_1\rangle = a_1|\psi_{12}^{+}\rangle|\psi_{34}^{+}\rangle + a_4|\varphi_{12}^{+}\rangle|\varphi_{34}^{+}\rangle, \\ |e_2\rangle = a_5|\psi_{12}^{-}\rangle|\psi_{34}^{-}\rangle + a_8|\varphi_{12}^{-}\rangle|\varphi_{34}^{-}\rangle.\end{aligned} \tag{B8}$$

Now we set $d=\sqrt{2}$ in Eqs. (B3) and (B4), which means $U_{23}|e_1\rangle = U_{14}|e_2\rangle$. This is the only one condition that further determines the coefficients $a_i(i=1,4,5,8)$. What we proceed with is a detailed expansion:

$$\begin{aligned}U_{23}|e_1\rangle &= \sqrt{2}\left\{\frac{1}{2}(|\uparrow\uparrow\rangle + e^{-i\phi'}|\downarrow\downarrow\rangle)(\langle\uparrow\uparrow| + e^{i\phi'}\langle\downarrow\downarrow|) + \frac{1}{2}(|\uparrow\downarrow\rangle - i|\downarrow\uparrow\rangle)(\langle\uparrow\downarrow| + i\langle\downarrow\uparrow|)\right\}_{23}\left\{\frac{a_1}{2}(|\uparrow\uparrow\rangle + e^{-i\phi'}|\downarrow\downarrow\rangle)_{12}(|\uparrow\uparrow\rangle\right. \\ &\left. + e^{-i\phi'}|\downarrow\downarrow\rangle)_{34} + \frac{a_4}{2}(|\uparrow\downarrow\rangle - i|\downarrow\uparrow\rangle)_{12}(|\uparrow\downarrow\rangle - i|\downarrow\uparrow\rangle)_{34}\right\} \\ &= |\psi_{23}^{+}\rangle\left\{\frac{a_1}{2}(|\uparrow\uparrow\rangle + e^{-i\phi'}|\downarrow\downarrow\rangle)_{14} + \frac{a_4}{2}(-i|\downarrow\downarrow\rangle - ie^{i\phi'}|\uparrow\uparrow\rangle)_{14}\right\} \\ &+ |\varphi_{23}^{+}\rangle\left\{\frac{a_1}{2}(e^{-i\phi'}|\uparrow\downarrow\rangle + ie^{-i\phi'}|\downarrow\uparrow\rangle)_{14} + \frac{a_4}{2}(-|\downarrow\uparrow\rangle + i|\uparrow\downarrow\rangle)_{14}\right\} \\ &= \frac{1}{2}(a_1 - ie^{i\phi'}a_4)|\psi_{23}^{+}\rangle|\psi_{14}^{+}\rangle + \frac{1}{2}(a_1e^{-i\phi'} + ia_4)|\varphi_{23}^{+}\rangle|\varphi_{14}^{-}\rangle,\end{aligned}$$

$$\begin{aligned}U_{14}|e_2\rangle &= \sqrt{2}\left\{\frac{1}{2}(|\uparrow\uparrow\rangle + e^{-i\phi'}|\downarrow\downarrow\rangle)(\langle\uparrow\uparrow| + e^{i\phi'}\langle\downarrow\downarrow|) + \frac{1}{2}(|\uparrow\downarrow\rangle - i|\downarrow\uparrow\rangle)(\langle\uparrow\downarrow| + i\langle\downarrow\uparrow|)\right\}_{23}\left\{\frac{a_5}{2}(|\uparrow\uparrow\rangle - e^{-i\phi'}|\downarrow\downarrow\rangle)_{12}(|\uparrow\uparrow\rangle\right. \\ &\left. - e^{-i\phi'}|\downarrow\downarrow\rangle)_{34} + \frac{a_8}{2}(|\uparrow\downarrow\rangle + i|\downarrow\uparrow\rangle)_{12}(|\uparrow\downarrow\rangle + i|\downarrow\uparrow\rangle)_{34}\right\} \\ &= |\psi_{23}^{+}\rangle\left\{\frac{a_5}{2}(|\uparrow\uparrow\rangle + e^{-i\phi'}|\downarrow\downarrow\rangle)_{14} + \frac{a_8}{2}(i|\downarrow\downarrow\rangle + ie^{i\phi'}|\uparrow\uparrow\rangle)_{14}\right\} \\ &+ |\varphi_{23}^{+}\rangle\left\{\frac{a_5}{2}(-e^{-i\phi'}|\uparrow\downarrow\rangle - ie^{-i\phi'}|\downarrow\uparrow\rangle)_{14} + \frac{a_8}{2}(-|\downarrow\uparrow\rangle + i|\uparrow\downarrow\rangle)_{14}\right\} \\ &= \frac{1}{2}(a_5 + ie^{i\phi'}a_8)|\psi_{23}^{+}\rangle|\psi_{14}^{+}\rangle + \frac{1}{2}(-a_5e^{-i\phi'} + ia_8)|\varphi_{23}^{+}\rangle|\varphi_{14}^{-}\rangle.\end{aligned} \tag{B9}$$

Because of the orthogonality of Bell states, we get the relation between coefficients

$$a_1 - ie^{i\phi'}a_4 = a_5 + ie^{i\phi'}a_8,$$

$$a_1e^{-i\phi'} + ia_4 = -a_5e^{-i\phi'} + ia_8,$$

$$\Rightarrow a_5 = -ie^{i\phi'}a_4, \quad a_8 = -ie^{-i\phi'}a_1. \tag{B10}$$

Setting $a_1 = \frac{1}{\sqrt{1+|\nu|^2}}$ and $a_4 = \frac{\nu}{\sqrt{1+|\nu|^2}}$, we finally arrive at

$$|e_1\rangle = \frac{1}{\sqrt{1+|\nu|^2}}(|\psi_{12}^{+}\rangle|\psi_{34}^{+}\rangle + \nu|\varphi_{12}^{+}\rangle|\varphi_{34}^{+}\rangle),$$

$$|e_2\rangle = \frac{-i}{\sqrt{1+|\nu|^2}}(\nu e^{i\phi'}|\psi_{12}^-\rangle|\psi_{34}^-\rangle + e^{-i\phi'}|\varphi_{12}^-\rangle|\varphi_{34}^-\rangle). \tag{B11}$$

They are indeed equivalent to Eq. (A16). The arbitrary parameter ν represents a certain degeneracy between the components of $|e_i\rangle$ with respect to the actions of U_{ij}. From the process of calculation, we can view U_{23} and U_{14} as the entanglement swapping operators on the pair-entangled states $|e_i\rangle$, in accord with the results in [13].

APPENDIX C: DECOMPOSITION OF $\check{R}(\theta)$

Here we give the proof of the decomposition (30) based on the work of Bullock and his coauthors [25,26]. They have developed the following criterion.

Proposition 1. An operator $u \in \mathrm{SU}(4)$ can be simulated using no CNOT gates and arbitrary one-qubit gates from SU(2) if and only if $\chi[\gamma(u)]=(x\pm 1)^4$. Here $\gamma(u)=u(\sigma_y \otimes \sigma_y)u^T(\sigma_y \otimes \sigma_y)$, u^T denotes the transpose, and $\chi[g]=\det[xI-g]$ denotes the characteristic polynomial of g.

Proposition 2. An operator $u \in \mathrm{SU}(4)$ can be simulated using one CNOT gate and arbitrary one-qubit gates from SU(2) if and only if $\chi[\gamma(u)]=(x+i)^2(x-i)^2$.

Proposition 3. An operator $u \in \mathrm{SU}(4)$ can be simulated using two CNOT gates and arbitrary one-qubit gates from SU(2) if and only if $\mathrm{tr}[\gamma(u)]=$ is real.

Direct calculation shows that the case $\theta=0$ satisfies proposition 1 while the case $\theta=\pi/4$ or $3\pi/4$ satisfies proposition 2. Since $\chi\{\gamma[\check{R}(\theta)]\}=(1+x^2-2x\cos 2\theta)$ and $\mathrm{tr}\{\gamma[\check{R}(\theta)]\}=4\cos 2\theta$, proposition 3 confirms that $\check{R}(\theta)$ generally admits a quantum circuit using two CNOT gates. The explicit form of V_i in Eq. (32) is calculated by the algorism in [25].

[1] C. N. Yang, Phys. Rev. Lett. **19**, 1312 (1967); Phys. Rev. **168**, 1920 (1968).

[2] R. J. Baxter, *Exactly Solved Models in Statistical Mechanics* (Academic, New York, 1982); Ann. Phys. (N.Y.) **70**, 193 (1972).

[3] For the collection of articles related to YBE, see, *Yang-Baxter Equation in Integrable Systems*, edited by M. Jimbo (World Scientific, Singapore, 1990); *Braid Group, Knot Theory and Statistical Mechanics*, 2nd ed., edited by C. N. Yang and M. L. Ge (World Scientific, Singapore, 1994).

[4] L. A. Takhtadzhan and L. D. Faddeev, Russ. Math. Surv. **34**, 11 (1979); L. D. Faddeev, Sov. Sci. Rev., Sect. C, Math. Phys. Rev. **C1**, 107 (1981); *Integrable Models in (1+1)-Dimensional Quantum Field Theory, Les Houches Lectures, 1982*, edited by J.-B. Zuber and R. Stora (North-Holland, Amsterdam, 1984); V. E. Korepin, N. M. Bogoliubov, and A. G. Izergin, *Quantum Inverse Scattering Method and Correlation Function* (Cambridge University Press, Cambridge, England, 1993).

[5] *The Many-Body Problem*, edited by D. C. Mattis (World Scientific, Singapore, 1993).

[6] D. A. Tennant, R. A. Cowley, S. E. Nagler, and A. M. Tsvelik, Phys. Rev. B **52**, 13368 (1995).

[7] V. F. R. Jones, Int. J. Mod. Phys. A **6**, 2035 (1991); M. L. Ge, K. Xue, and Y. S. Wu, *ibid.* **6**, 3735 (1991).

[8] A. Y. Kitaev, Ann. Phys. (N.Y.) **303**, 2 (2003); M. H. Freedman, A. Y. Kitaev, and Z. H. Wang, Commun. Math. Phys. **227**, 587 (2002); H. A. Dye, Quantum Inf. Process. **2**, 117 (2003).

[9] L. H. Kauffman and S. J. Lomonaco, Jr., New J. Phys. **6**, 134 (2004).

[10] Y. Zhang, L. H. Kauffman, and M. L. Ge, Int. J. Quantum Inf. **3**, 669 (2005).

[11] J. M. Franko, E. C. Rowell, and Z. Wang, J. Knot Theory Ramif.. **15**, 413 (2006).

[12] Y. Zhang and M. L. Ge, Quantum Inf. Process. **6**, 363 (2007).

[13] J. L. Chen, K. Xue, and M. L. Ge, Phys. Rev. A **76**, 042324 (2007).

[14] Y. Zhang, E. C. Rowell, Y. S. Wu, Z. H. Wang, and M. L. Ge, e-print arXiv:0706.1761.

[15] E. Ardonne and K. Schoutens, Ann. Phys. **322**, 201 (2007); A. Feiguin, S. Trebst, A. W. W. Ludwig, M. Troyer, A. Kitaev, Z. H. Wang, and M. H. Freedman, Phys. Rev. Lett. **98**, 160409 (2007); for a review, see, C. Nayak, S. H. Simon, A. Stern, M. Freedman, and S. D. Sarma, e-print arXiv:0707.1889; K. Hikami, Ann. Phys. **323**, 1729 (2008).

[16] P. Kok, W. J. Munro, K. Nemoto, T. C. Ralph, and P. Jonathan, Rev. Mod. Phys. **79**, 135 (2007).

[17] J. L. O'Brien, G. J. Pryde, A. G. White, T. C. Ralph, and D. Branning, Nature (London) **426**, 264 (2003).

[18] F. Wilczek, Phys. Rev. Lett. **48**, 1144 (1982); G. Moore and N. Read, Nucl. Phys. B **360**, 362 (1991).

[19] H. N. V. Temperley and E. H. Lieb, Proc. R. Soc. London, Ser. A **322**, 251 (1971).

[20] N. J. Cerf, C. Adami, and P. G. Kwiat, Phys. Rev. A **57**, R1477 (1998).

[21] B. G. Englert, C. Kurtsiefer, and H. Weinfurter, Phys. Rev. A **63**, 032303 (2001).

[22] J. Lu, L. Zhou, and L. M. Kuang, Phys. Lett. A **330**, 48 (2004).

[23] *Polarized Light (Benchmark Papers in Optics, 1)*, edited by W. Swindell (Dowden, Hutchinson, and Ross, Stroudsburg, 1975).

[24] G. M. D'Ariano and P. Lo Presti, Phys. Rev. Lett. **86**, 4195 (2001).

[25] S. S. Bullock and I. L. Markov, Phys. Rev. A **68**, 012318 (2003).

[26] V. V. Shende, S. S. Bullock, and I. L. Markov, Phys. Rev. A **70**, 012310 (2004).

[27] E. Knill, R. Laflamme, and G. Milburn, Nature (London) **409**, 46 (2001).

[28] T. C. Ralph, Phys. Rev. A **70**, 012312 (2004).